ECS Journal of Solid State
Science and Technology

Integrated Energy Conversion and Storage Device for Stable Fast Charging Power Systems

To cite this article before publication: Jihun Kim *et al* 2020 *ECS J. Solid State Sci. Technol.* in press https://doi.org/10.1149/2162-8777/abcc49

Integrated Energy Conversion and Storage Device for Stable Fast Charging Power Systems

Journal:	*ECS Journal of Solid State Science and Technology*
Manuscript ID	JSS-100680.R1
Manuscript Type:	Research Paper
Date Submitted by the Author:	09-Nov-2020

Complete List of Authors:	Kim, Jihun; Gwangju Institute of Science and Technology Park, Hyeonghun; Gwangju Institute of Science and Technology, Jang, Junsung; Chonnam National University Song, Hyeongi; Gwangju Institute of Science and Technology Lee, Byeong Hoon; Chonnam National University Lee, Dongmin; Chonnam National University Jang, Suyoung; Chonnam National University Kim, Jin Hyeok; Chonnam National University Kim, Hyeong-Jin; Gwangju Institute of Science and Technology,

Keywords:	Energy Conversion - Photovoltaics, Energy Storage, Batteries – Li-ion, Hybrid Solar Battery

Integrated Energy Conversion and Storage Device for Stable Fast Charging Power Systems

Jihun Kim,[1] Hyeonghun Park,[1] Junsung Jang,[2] Hyeongi Song,[1] Byeong Hoon Lee,[2] Dongmin Lee,[2] Suyoung Jang,[2] Jin Hyeok Kim,[2,z] and Hyeong-Jin Kim[1,*,z]

[1]School of Integrated Technology, Gwangju Institute of Science and Technology, Buk-gu, Gwangju 61005, Republic of Korea

[2]Optoelectronic Convergence Research Center and Department of Materials Science and Engineering, Chonnam National University, Buk-gu, Gwangju 61186, Republic of Korea

*Electrochemical Society Member.

[z]E-mail: hjkimc@gist.ac.kr; jinhyeok@chonnam.ac.kr

Abstract

Herein, an integrated device that comprises inorganic kesterite solar cells and Li-ion batteries (LIBs) has been proposed for application in fast photo-charging power systems. $LiFePO_4$ and $Li_4Ti_5O_{12}$ were selected as the battery electrode materials and six kesterite solar cells connected in series were fabricated to satisfy the charging voltage required for LIBs. Photo-charging was conducted at the rate of 1 C (1.790 mAh/g) at 2.1 V. An energy conversion and storage efficiency of 3.87% was acquired in the integrated device, and a storage efficiency of over 70% was observed in LIBs. Furthermore, by synchronizing the charging voltage of the solar cell and LIB, over 70% of the capacity was obtained at the rate of 1 C, while preventing overvoltage during long-term charging.

This paper is part of the JSS Focus Issue on Photovoltaics for the 21st Century.

Introduction

Solar power is the most abundant renewable energy source, and the direct charging approach is necessary for the development of next-generation power systems. As demand for the efficient storage of energy using renewable resources increases, the interest in research on devices incorporating solar cells and batteries is also amplifying. Accordingly, relevant research is currently being conducted according to different types of materials and electrodes that are used in solar cells and batteries [1-6]. Consequently, integrated device systems with energy conversion and storage efficiencies (ECSEs) of approximately 10% have already been reported [7]. For a high ECSE, solar cells based on perovskites, dyes, and silicon, are frequently used. Furthermore, studies based on lithium ion batteries (LIBs) have been conducted due to their high specific capacity and stability [8-10].

Gurung et al. reported a charging system based on a perovskite solar cell-converter using LIB. In the study, a DC-DC voltage converter was used to obtain a sufficient voltage for a single solar cell to charge the LIB [11]. The device demonstrated a notable ECSE of 9.36% and an average storage efficiency of over 75% at a discharge rate of 0.5 C [11]. Weng et al. deposited n-i-p type perovskite solar cells on the electrodes of either aqueous lithium or

sodium (Li/Na)-ion batteries by employing an asphalt-derived carbon coating method to significantly improve the rate performance [7]. The photovoltaic battery system achieved ECSE of 9.3% at a discharge rate of 2 C, with a stable cycling performance for around 40 cycles [7]. Um and Choi et al. reported a monolithically integrated and photo-rechargeable portable power system based on crystalline Si photovoltaic modules and solid-state LIBs [12]. In particular, a solid-state LIB is integrated directly on the aluminum electrode of a c-Si photovoltaic (PV) module via an in-series printing process [12]. The integrated device exhibited an ECSE of 7.61% when subjected to rapid charging for less than 2 min, while exhibiting a high-performance rate capability of 28 C [12]. The GM research group directly tested the solar photovoltaic charging of batteries using Si PV and LIB modules as a proof of concept for solar PV charging of batteries to develop electrically powered vehicles [10]. In this result, the ECSE reached a value of 14.5% with a battery charging efficiency of approximately 100% without any intervening electronics, while matching the maximum PV power point voltage to the battery charging voltage [10].

The integrated device can be configured according to the design of the electrode. Depending on the design of the electrode, energy storage efficiency can be improved, and the configuration can be simplified. The design methods can be characterized into two approaches, namely: simply connecting a solar cell and a battery along with an electrode or designing a bi-functional electrode [8, 13-17]. In the case of the bi-functional electrode, a reversible reaction occurs and a material capable of generating light is used as an electrode to simultaneously produce and store energy. Hu et al. demonstrated a portable solar-rechargeable electric energy storage system using a bifunctional aluminum electrode without an external circuit [8]. They interconnected three identical perovskite solar module on the same substrate and directly assembled an aluminum ion battery on the outer most perovskite solar module aluminum electrode [8]. The integrated device exhibited a high power density of 5000 W/kg and energy density of 43 Wh/kg [8]. By rationally matching the maximum power point voltage of solar module and battery, notable high photoelectric conversion and storage efficiency of 12.04% can be achieved [8]. Yu et al. reported a built-in dye-sensitized titanium dioxide photoelectrode with photo-assisted charging of a lithium-oxygen battery [17]. They demonstrated that the photoelectrode reduced the charging overpotential due to the generation of a photovoltage that arises as an effect of the redox shuttle [17]. It is noticeable that the charging voltage reduced over the O_2/Li_2O_2 redox potential (+2.96 V), which is thermodynamically impossible by the contribution of a solar energy input [17]. Li et al. investigated a solar-driven chargeable lithium-sulfur battery with a Pt-modified CdS photocatalyst [14]. The cathode in the integrated device plays the bi-functional role of photo-charging and energy storage [14]. In addition, the photocatalyst in the cathode generated hydrogen by water splitting [14]. The integrated device deliver a specific capacity of 792 mAh/g during a photo-charging process of 2 h, with a discharging potential of approximately 2.53 V(vs Li+/Li) [14]. Recently, Gurung et al. reported the fully integrated device by using monolithic stacking approach of the battery on the solar cell using a common metal substrate. The integrated device exhibited the high ECSE of 7.3% with maximum power point tracking system [15].

In order to utilize the integrated device as a next-generation power supply, it is necessary to increase its ECSE and lower the fabrication cost. In this study, integrated devices have

been prepared by using an inorganic kesterite solar cell, which is composed of low-cost elements; this is aimed at increasing the stability and lowering the cost of energy production when using LIBs. Direct connection was conducted using metal wires which is simple and facile way to realize integrated device. When charging the energy of a battery using a solar cell, matching the output voltage of the solar cell with the battery discharge voltage can lead to overvoltage prevention. The safe operation of the integrated device was observed, which exhibited a storage efficiency of over 70% and prevented overvoltage even when overcharged. The proposed device showed a charge rate of 72% when compared to that of the original capacity by minimizing the loss in capacity due to voltage matching. Above all, here the approach using low cost inorganic kesterite solar cells is proposed for the first time.

Experimental

1. CZTSSe solar cells

CZTSSe solar cells were deposited by a direct-current (DC) based sputter process in a high-vacuum chamber. A Zn/Sn/Cu ordered stack metallic precursor was prepared with a sputtering power density of 0.65 W/cm^2 under the base pressure of 10^{-4} Pa. The precursors were annealed for sulfurization in a graphite box in the presence of S (0.0019 mg) and Se (0.198 mg) by using a rapid thermal annealing system. A cadmium sulfide (CdS) buffer layer was then grown by a chemical bath deposition method at a temperature of 60 ℃ for 14 min. Intrinsic ZnO, Al-doped ZnO (AZO) transparent electrode, and Al top electrode, were formed via sputtering.

2. LFP-LTO battery

$LiFePO_4$ (LFP) electrode slurry was composed of 90 wt% $LiFePO_4$, 5 wt% acetylene black and polyvinylidene fluoride (PVDF) with N-methyl pyrrolidone (NMP). $Li_4Ti_5O_{12}$ (LTO) electrode slurry was composed of 90 wt% $Li_4Ti_5O_{12}$, 5 wt% acetylene black and PVDF with NMP. Each slurry was mixed by performing planetary ball milling for 4 h at a speed of 400 rpm. The LFP slurry was coated onto an Al foil with the loading density of 6.88 mg/cm^2, and the LTO slurry was coated onto a Cu foil with the loading density of 7.08 mg/cm^2 using the doctor blade coating process. The LIBs were fabricated as 2032-type coin cells in an Ar-filled glove box. Ethylene carbonate/diethyl carbonate (1:1 v/v) and 1M of lithium hexafluorophosphate were used for an electrolyte. Polypropylene was used as the separator.

3. Characterization

Current-voltage curves of solar cells were acquired from a Xe light source-based solar simulator (Sol3A, Oriel, USA) under standard conditions (AM 1.5G radiation, 100 mW/cm^2, 25 ℃). Galvanostatic charge/discharge and capacity properties were measured using a battery cycler (WBCS 3000, Wonatech, Korea) at a potential range of 1.0-2.6 V (vs Li+/Li) for various C-rates ranging from 0.1 to 2 C.

Results

As a major component of the integrated device, the solar cell was manufactured to comprise a structure of Mo/CZTSSe(~1.5 um)/CdS(40 nm)/i-ZnO(60 nm)/AZO(600 nm)/Al(1 um). CZTSSe solar cell is essentially an inorganic base, thereby exhibiting chemical and thermal stabilities and good long-term cyclability. In addition, it has a high short-circuit current, which enables rapid charging. However, in order to match the charging voltage of the battery with the output voltage of the solar cell, it is necessary to configure the

solar cells in a series or a module due to their low open circuit voltage. Therefore, six kesterite solar cells were fabricated and connected in series to satisfy the charging voltage of the battery. Figure 1 and table 1 represent the current-voltage (*I-V*) curves and details for the series-connected kesterite solar cell and single solar cell, which exhibited a power conversion efficiency (PCE) of 5.8% with an open circuit voltage of 2.9 V in series-connected cell. Further, it comprised a short-circuit current of 8.98 mA and a fill factor (*FF*) of 43%. Although the open circuit voltage increased sufficiently to charge a battery, the short circuit current correspondingly decreased due to a mismatched current of solar cells. Although the efficiency of the solar cell is low, it is necessary to lower the output current of the solar cells in order to charge the coin cell type battery at an appropriate C-rate. The solar cells were selected to achieve a rate of 1 C (1.790 mAh) at 2 V. During the charging process, the three-coin cells were simultaneously charged to achieve a current corresponding to 1 C.

$LiFePO_4$ (LFP) and $Li_4Ti_5O_{12}$ (LTO) were selected as active materials of the electrodes for achieving stability, a high energy density, and excellent repeatability. Figure 2 shows the rate capability, galvanostatic charge/discharge, and Coulombic efficiencies for the LTO-Li half-cell and the LTO-LFP full cell. The half-cell recorded a capacity of 163 mAh/g in the initial charge/discharge stage, which is shown in figure 2(a). The LTO half-cell showed a typical charge/discharge curve in the Figure 2 (b) and exhibited an excellent rate performance, while achieving the high capacity of 157 mAh/g even at 2 C. The charge voltage plateau was found to be 1.6 V and the Coulombic efficiency was over 98%, as observed in Figure 2 (c). The Coulombic efficiency of more than 100% is a result of the overcharging due to the presence of Li-metal. In the full cell, a charging capacity of 142 mAh/g was determined at 0.1 C, when considering a decrease in the charging capacity for stabilization. As the C-rate increased, the charging capacity decreased gradually, and the charging capacity of 126, 100, 86, 60 mAh/g was observed at 0.2 C, 0.5 C, 1 C and 2 C, respectively (Figure 2 (d)). In Figure 2 (e), the galvanostatic charge/discharge test was performed in the full cell in the voltage range of 1-2.6 V, and it exhibited a typical charge/discharge curve according to the C-rate. A plateau appeared at 2 V and a comparatively low overvoltage was observed. The rise of the voltage plateau according to the C-rate was up to 2.4 V. In Figure 2 (f), Coulomb efficiency can be determined depending on the C-rate. The full cell consistently achieved a coulomb efficiency of over 98% at 1 C.

After the solar cell-battery integrated device was photo-charged with a light energy density of 100 mW/cm^2, which corresponds to AM 1.5, a galvanostatic charge/discharge process was performed using a battery test system. A charge/discharge test was conducted by wiring the series-connected solar cell and the coin cell type battery which is shown in Figure 3 (a) and (b) as photo and schematic images. In photo image, six LIBs were charging yet in this study three LIBs were used to match the rate of 1 C. Photo-charging proceeded for 1 h and the charging conditions corresponded to 1 C (1.790 mA). Figure 4 (a-c) represents the delivered and charged energies with respect to the battery. In the initial stage, a capacity of 71.4 mAh/g was exhibited, corresponding to 82% (86.4 mAh/g) of the capacity at the rate of 1 C. Further, it was confirmed that even after repeated operation cycles, the integrated device operated stably without any further decrease in capacity (Figure 4 (a)). When employing existing organic material-based solar cells, the discharge efficiency decreases with repeated operation due to environmental vulnerability; however, inorganic material-based kesterite

solar cells showed long-term stability (Figure 4 (b)). In a 20-cycle operation, over 95% retention of the PCE was shown in the kesterite solar cell.
ECSE and storage efficiency are used to evaluate the efficiency of integrated devices and batteries. ECSE can be calculated as follows [11].

$$\eta_1 = E_{discharge} / (P \times A \times t) \times 100\% \quad (1)$$

where $E_{discharge}$, P, A, and t are discharge energy delivered to LIBs (mWh), light power density (100 $mWcm^{-2}$), solar cell area (cm^{-2}) and the photo-charge time (h), respectively [11]. The storage efficiency for photo-charged LIB can be calculated as follows.

$$\eta_2 = \eta_1 / \eta_{solar} \times 100\% \quad (2)$$

where η_{solar} is the conversion efficiency of solar cells. In Figure 4 (c), the ECSE and storage efficiency of the integrated device and battery can be confirmed, depending on the number of operation cycles. The integrated device exhibited an ECSE of 3.87%, which was maintained consistently during 20 operation cycles. The storage efficiency in the battery achieved a value of 70% at 1 C. Even when the cycles were repeated again for 10 times, the storage efficiency of 70% was retained, thereby showing a stable driving environment. A notably high percentage of the electrical energy converted through photo-charging was stored in the battery. Although the conversion efficiency of the integrated device exhibited a relatively low value, the storage efficiency was recorded to be high. Furthermore, a high ECSE was observed when comparing the low efficiency of the solar cell at a high rate of 1 C. Here, the development of an energy conversion and storage system that is capable of fast charging has been achieved because the integrated device is based on a stable material; further, this approach has shown the possibility of the system enabling increasing charging efficiency. However, integrated system using Li-metal based batteries with a high theoretical capacity and long-term stability demonstrating from state-of-the art technology such as bi-layer for protection are strong candidate for the energy conversion and storage system [18]. It can be considered as a next-generation high capacity and stable power system by combining with CZTSSe solar cell which exhibits the excellent stability.

Incorporating a battery into a solar cell enables efficient energy conversion and storage; however, safety issues must also be addressed. When the battery is charged at a voltage that exceeds the rated value, an overvoltage may arise, thereby facilitating the damage and ignition of the battery system. To solve this problem, the charging voltages of the solar cell and the battery can be synchronized. If the charging voltage of the solar cell is set to be below the voltage at which the overvoltage appears in the battery, the battery could be safely operated even for a long-term charging process. However, when the charging voltage is lower than that of the battery, battery cannot be fully charged. Therefore, it is necessary to implement a system that safely transfers a large amount of electrical energy by precisely synchronizing the voltage from both devices. In this study, it has been observed that the stable operation of the LFP-LTO battery is possible at a voltage range of 2-2.5 V. The charging process was performed by setting the maximum charging voltage of the solar cell to 2.9 V. Figure 5 shows the specific discharge capacity of the battery depending on the charging time. As can be seen from the graph, the capacity does not increase proportionally to

time, and charging gradually stops after a certain time. For the initial 1h charging process, a capacity of 62.7 mAh/g was exhibited. At 40 min, a capacity of 50.6 mAh/g was obtained, and at 3h, a capacity of 64.4 mAh.g; these results were obtained at the charging condition of 1 C. At 5 h, a capacity of 68.0 mAh/g was obtained, which is almost similar to that observed after charging for 3 h; further, no damage was caused to the battery even after a long-term operation. When charged by a power supply at 1 C, a capacity of 86.1 mAh/g was observed. It was confirmed that 72% of the capacity was delivered from the integrated device when charged using a power supply. Thus, this approach can be used to develop a system that can stably produce energy and safely store it with its high capacity.

Conclusions [Required]

In this study, integrated devices have been prepared using inorganic kesterite solar cells and LFP-LTO-based LIBs. In order to satisfy the charging voltage of the battery, six series type kesterite solar cells were fabricated; subsequently, they were wired with batteries. The solar cell connected in series showed a conversion efficiency of 5.8% with an oven circuit voltage of 2.9 V. The LFP-LTO battery exhibited a specific capacity of 86 mAh/g at 1 C. In the fast charging condition, the energy conversion and storage efficiency of the integrated device was 3.87%, which was confirmed by the photo-charged cells that exhibited a capacity of 68 mAh/g at the rate condition of 1C; further, the storage efficiency of the battery was high at 70%. By synchronizing the charging voltages of the solar cell, and battery a capacity of over 70% was achieved, while preventing overvoltage even after long-term charging. As a result, a solar cell-battery integrated device system that can be safely driven with high storage efficiency has been proposed.

Acknowledgments

This research was financially supported by the GIST Research Institute (GRI) grant funded by the GIST in 2020 and the Korea Institute of Energy Technology Evaluation and Planning(KETEP) and the Ministry of Trade, Industry & Energy(MOTIE) of the Republic of Korea (No.: 20194030202470 and 20204010600340).

References

1. Y. Yuan, Y. Lu, B.-E. Jia, H. Tang, L. Chen, Y.-J. Zeng, Y. Hou, Q. Zhang, Q. He, L. Jiao, J. Leng, Z. Ye, J. Lu, *Nano-Micro Lett.* **11**, (1), 42 (2019).
2. C. Li, S. Cong, Z. Tian, Y. Song, L. Yu, C. Lu, Y. Shao, J. Li, G. Zou, M. H. Rümmeli, S. Dou, J. Sun, Z. Liu, *Nano Energy* **60**, 247-256 (2019).
3. J. Xu, Y. Chen, L. Dai, *Nat. Commun.* **6**, (1), 8103 (2015).
4. W. Li, H.-C. Fu, L. Li, M. Cabán-Acevedo, J.-H. He, S. Jin, *Angew. Chem. Int. Ed.* **55**, (42), 13104-13108 (2016).
5. A. Hauch, A. Georg, U. O. Krašovec, B. Orel, *J. Electrochemical Soc.* **149**, (9), A1208 (2002).
6. Y.-H. Lee, J.-S. Kim, J. Noh, I. Lee, H. J. Kim, S. Choi, J. Seo, S. Jeon, T.-S. Kim, J.-Y. Lee, J. W. Choi, *Nano Lett.* **13**, (11), 5753-5761 (2013).
7. G.-M. Weng, J. Kong, H. Wang, C. Karpovich, J. Lipton, F. Antonio, Z. S. Fishman, H. Wang, W. Yuan, A. D. Taylor, *Energy Storage Mater.* 24, 557-564 (2020).
8. Y. Hu, Y. Bai, B. Luo, S. Wang, H. Hu, P. Chen, M. Lyu, J. Shapter, A. Rowan, L. Wang, *Adv. Energy Mater.* **9**, (28), 1900872 (2019).

9. W. Guo, X. Xue, S. Wang, C. Lin, Z. L. Wang, *Nano Lett.* **12**, (5), 2520-2523 (2012).
10. T. L. Gibson, N. A. Kelly, 2009 *IEEE Vehicle. Power*, **7**, 310-316 (2009).
11. A. Gurung, K. Chen, R. Khan, S. S. Abdulkarim, G. Varnekar, R. Pathak, R. Naderi, Q., Qiao, *Adv. Energy Mater.* **7**, (11), 1602105 (2017).
12. H.-D. Um, K.-H. Choi, I. Hwang, S.-H. Kim, K. Seo, S.-Y. Lee, *Energy Environ. Sci.* **10**, (4), 931-940 (2017).
13. A. Gurung, Q. Qiao, *Joule* **2**, (7), 1217-1230 (2018).
14. N. Li, Y. Wang, D. Tang, H. Zhou, *Angew. Chem. Int. Ed.* **54**, (32), 9271-9274 (2015).
15. A. Gurung, K. M. Reza, S. Mabrouk, B. Bahrami, R. Pathak, B. S. Lamsal, S. I. Rahman, N. Ghimire, R. S. Bobba, K. Chen, J. Pokharel, A. Baniya, M. A. R. Laskar, M. Liang, W. Zhang, W. -H. Zhang, S. Yang, K. Xu, Q. Qiao, *Adv. Funct. Mater.* **30**, 2001865 (2020)
16. A. Paolella, C. Faure, G. Bertoni, S. Marras, A. Guerfi, A. Darwiche, P. Hovington, B. Commarieu, Z. Wang, M. Prato, M. Colombo, S. Monaco, W. Zhu, Z. Feng, A. Vijh, C. George, G. P. Demopoulos, M. Armand, K. Zaghib, *Nature Commun.* **8**, (1), 14643 (2017).
17. M. Yu, X. Ren, L. Ma, Y. Wu, *Nature Commun*. **5**, (1), 5111 (2014).
18. R. Pathak, K. Chen, A. Gurung, K. M. Reza, B. Bahrami, F. Wu, A. Chaudhary, N. Ghimire, B. Zhou, W. -H. Zhang, Y. Zhou, Q. Qiao, *Adv. Energy Mater.* **9**, (36), 1901486 (2019)

Figures

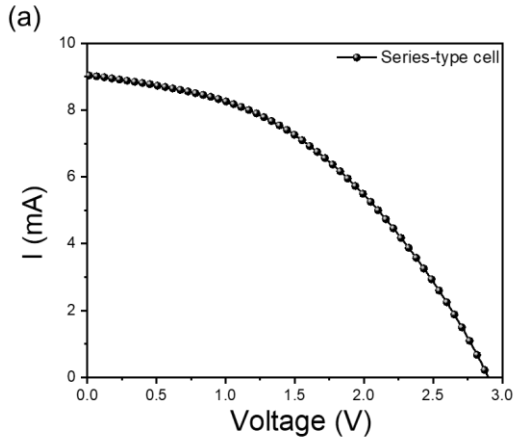

Figure 1. *I-V* curves of the series-type kesterite solar cell and single solar cell.

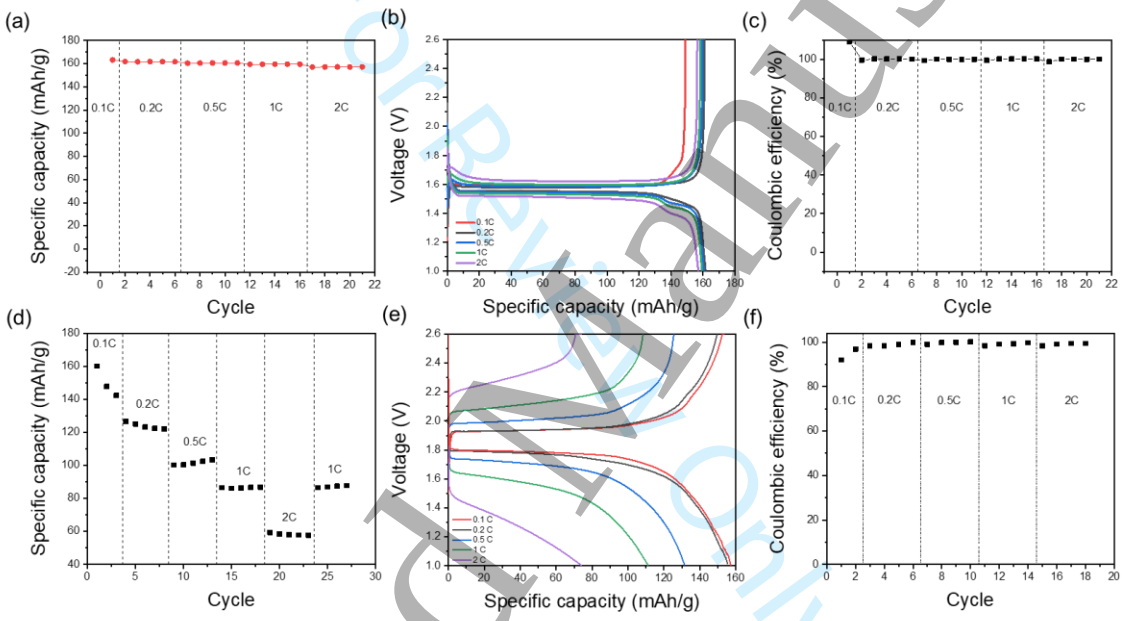

Figure 2. (a) Rate performance, (b) galvanostatic charge/discharge curves and (c) Coulombic efficiency for LFP-Li metal half-cell and (d) Rate performance, (e) galvanostatic charge/discharge curves and (f) Coulombic efficiency for LFP-LTO full cell.

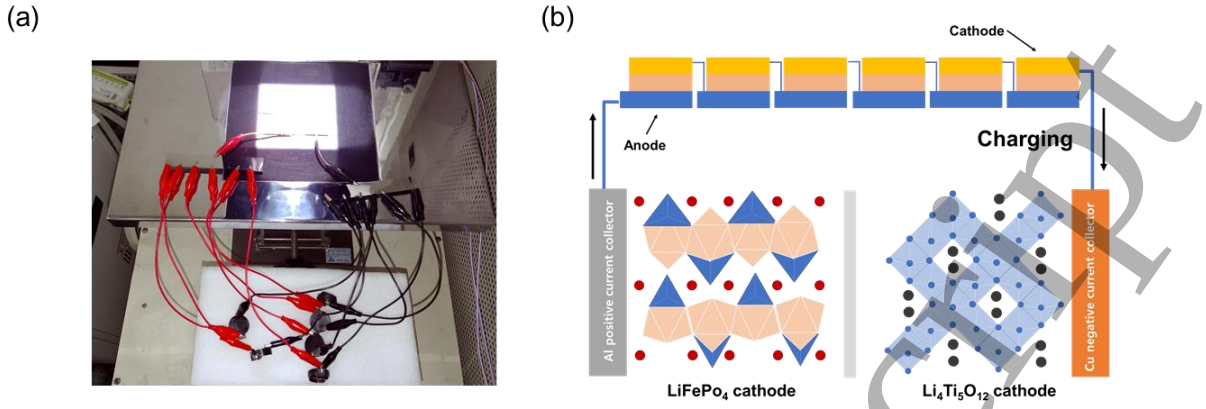

Figure 3. (a) Photo and (b) schematic images of photo-charging using kesterite solar cell and li-ion batteries.

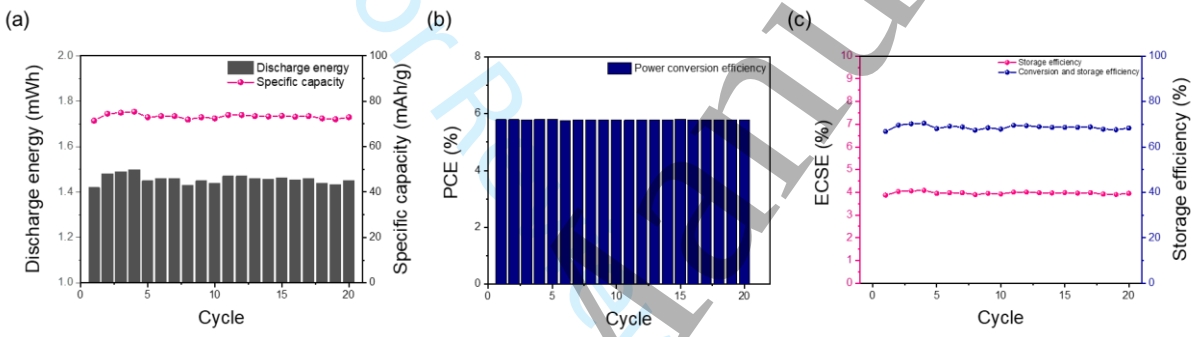

Figure 4. (a) Discharge energy and specific capacity versus cycle number of photo-charged LIBs. (b) PCE versus cycle number of the series-connected kesterite solar cell. (c) ECSE and storage efficiency versus cycle number.

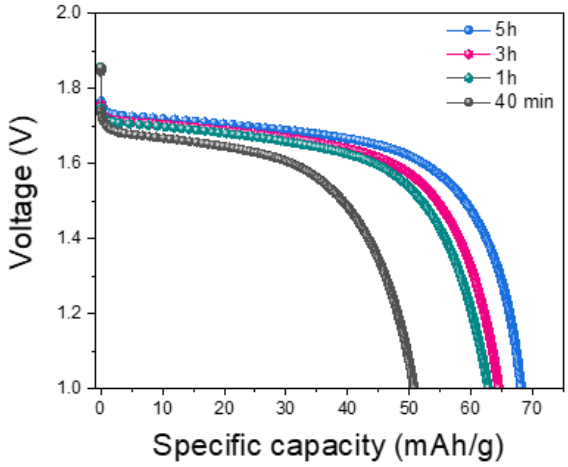

Figure 5. Discharge curves depending on photo-charging time.

Table

	V_{oc} (V)	I_{sc} (mA)	*FF* (%)	η (%)	R_s (Ω, series resistance)
Series-type cell	2.90	8.98	43	5.80	115
Single cell	0.44	12.16	40	7.29	17

Table 1. *I-V* curve details of the series-type kesterite solar cell and single cell.